Proceedings of the 1st Marine Energy Technology Symposium
METS13
April 10-11, 2013, Washington, D.C.

COMBINING MULTI-BODY DYNAMICS AND POTENTIAL FLOW SIMULATION METHODS TO MODEL A WAVE ENERGY CONVERTER

Chris McComb[1]
Carnegie Mellon University
Pittsburgh, PA, USA

Michael Lawson
National Renewable Energy Laboratory
Golden, CO, USA

Yi-Hsiang Yu
National Renewable Energy Laboratory
Golden, CO, USA

[1]Corresponding author: chris.c.mccomb@gmail.com

ABSTRACT

Numerical simulations that predict the dynamics and performance of wave energy converters (WECs) require the simulation of complex fluid-structure interactions between a WEC device and the wave environment. Navier-Stokes computational fluid dynamics (CFD) simulations and fully time-domain boundary integral equation methods (BIEMs) can be coupled with multi-body dynamics solvers to simulate these problems. However, the computational resources that are required to perform these types of high-fidelity simulations are significant, precluding the use of CFD and time-domain BIEM for design optimization. One method for reducing the numerical complexity of WEC simulations is to model the hydrodynamics using frequency-domain simulations, while model the dynamic motion of the WEC device in the time-domain using multi-body dynamics methods.

The primary objective of the work presented herein is to develop such a numerical tool using the multi-body solver SimMechanics and the frequency-domain hydrodynamics code WAMIT. The numerical tool was developed so that WEC devices comprised of arbitrarily connected bodies, power-take-off (PTO) systems, and mooring systems can be simulated in operational sea states, where the wave environment can be modeled under linear assumptions. The remainder of this paper describes the development and verification of the numerical tool.

INTRODUCTION

WEC devices were patented as early as the 1800s, but development efforts remained generally dormant until the last several decades, when renewable energy technologies experienced renewed interest [1]. Recent research indicates that on average there is approximately 3 TW of extractable wave energy contained within the world's oceans [2], suggesting WEC technologies could provide significant contributions to the worlds growing energy demands. Besides offering a significant contribution to a diverse renewable energy portfolio, wave energy also offers several potential benefits over other renewable energy sources. These benefits include seasonable predictability and high resource availability near the coastal population centers of the world [1] [2].

Despite the growing interest in wave energy, unresolved problems still exist with the design and analysis of WEC technologies. These unresolved problems include optimal design for robustness across a range of sea states, power-take-off (PTO) design and control optimization, and determination of loads during survival conditions.

A variety of numerical methods have been developed for the simulation of WECs. Many of these have been adapted from methods already proven in other offshore applications. The most common categories are analytical methods, empirical methods, Navier-Stokes equation methods (NSEMs) and boundary-integral equation methods (BIEM). Analytical methods offer quick and rough estimates for devices with simple geometry. Many empirical methods maintain the simplicity of the analytical methods, but make use of experimental values in an attempt to increase accuracy. Navier-Stokes equation methods can resolve highly nonlinear phenomena, but are very computationally expensive. Methods of this type are generally referred to as computational fluid dynamics (CFD) methods. BIEM is another commonly used numerical method, which produces a potential theory solution and are well suited to more complicated geometry.

Given that fully time-domain BIEM can be computationally expensive, solving the frequency domain radiation and diffraction problems is a commonly used method of reducing the numerical complexity of WEC simulations. The method determines hydrodynamic forces based on frequency-domain BIEM simulation and models the motion of the WEC device in the time-domain using multi-body dynamics methods. Frequency-domain BIEM is far less computationally expensive than NSEM and fully time-domain BIEM, and for this reason the method is well suited for performing rapid design iterations and optimization [4][5].

The numerical tool that is described in this paper uses frequency-domain BIEM in conjunction with multi-body dynamics simulations. SimMechanics was chosen as the multi-body dynamics solver because it readily interfaces with MATLAB Simulink, a program commonly used to simulate control systems, although control strategies were not explored.

This paper first describes the composition of the generic two-body point absorber WEC used in this study. Next, we describe the physics-based mathematical model we developed to describe the behavior and performance of the WEC device. The numerical implementation of the mathematical models is then outlined. Finally, the model is verified by comparison to analytical solutions and is used to predict power output for a WEC device deployed at a wave energy site near Hanstholm, Denmark.

WAVE ENERGY CONVERTER COMPOSITION

All simulations described in this paper were conducted with the WEC shown in Figure 1. This WEC is a two-body floating-point absorber. Relevant parameters and dimensions associated with the WEC are shown in Table 1. The parameters associated with the PTO system are discussed in more detail in the System Dynamics section.

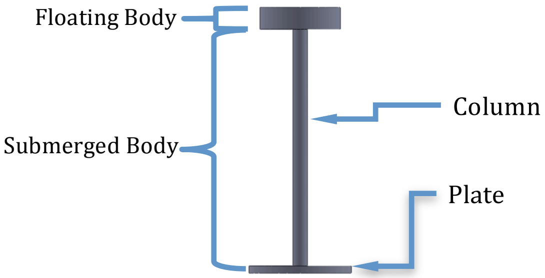

FIGURE 1. TWO-BODY FLOATING-POINT ABSORBER

TABLE 1. PARAMETERS FOR THE POINT ABSORBER.

Parameter	Value
Floating Body	
Diameter	11.0 m
Height	3.0 m
Mass	86 ton
Viscous drag coefficient	1.0
Submerged Body	
Column	
Diameter	2.0 m
Height	32.0 m
Plate	
Diameter	14.0 m
Height	1.0 m
Mass	260 ton
Viscous drag coefficient	3.0
Power Take-Off System	
Damping coefficient	1200 kNs/m
Stiffness coefficient	0.0 kN/m

MATHEMATICAL DESCRIPTIONS

The WEC modeling tool was developed by using frequency-domain BIEM methods to determine hydrodynamic loads and solving the Cummins equation [6] to determine the time-domain motions and loads on the WEC device,

$$\boldsymbol{M\ddot{X}} = \boldsymbol{F_{ex}} + \boldsymbol{F_{rad}} + \boldsymbol{F_{PTO}} + \boldsymbol{F_{v}} + \boldsymbol{F_{B}} \tag{1}$$

where $\boldsymbol{\ddot{X}}$ is the (translational and rotational) acceleration of the device. $\boldsymbol{M}$ is the mass matrix, $\boldsymbol{F_{ex}}$ is the wave excitation forces, $\boldsymbol{F_{rad}}$ is the force vector due to wave radiation, $\boldsymbol{F_{PTO}}$ is the PTO force, $\boldsymbol{F_{v}}$ is the viscous force, and $\boldsymbol{F_{B}}$ was the buoyancy restoring force. For simplicity, the forces induced by mooring and the coriolis force were not considered in this numerical model. The remainder of this section describes each of these force calculations in further detail.

Hydrodynamic Coefficients

For calculating the hydrodynamic forcing terms in Eq. (1), the radiation and diffraction problems were solved using WAMIT [7], a frequency-domain BIEM, to obtain the wave excitation, added-mass and radiation damping coefficients. The solution consists of two cases. In the radiation case, the body is forced to oscillate harmonically at the frequency of the incident waves. From this case, radiation damping and added mass coefficients are determined. Next, the body is fixed at the mean position and made subject to incident waves. This diffraction case determines the excitation forces on the body, including the wave load due to wave diffraction.

The added mass and radiation damping coefficients are defined in terms of a surface integral that returns a complex value [7].

$$A_{ij} - \frac{i}{\omega} B_{ij} = \rho \iint_{S_b} n_i \varphi_j dS \tag{2}$$

where ω is the frequency of the incident wave, ρ is water density, φ_j is the unit-amplitude radiation potential, n_j is the appropriate component of the surface normal vector, A_{ij} is the added mass, and B_{ij} is the radiation damping coefficient.

The excitation vector term is defined as a phasor, indicating the magnitude and the phase of the sinusoidal force. This vector can be calculated through direct integration of the hydrodynamic pressure [7],

$$\boldsymbol{FX} = -i\omega\rho \iint_{S_b} \boldsymbol{n}\varphi_D dS \tag{3}$$

where $\boldsymbol{n}$ is the surface normal vector, and φ_D is the velocity potential solved in the diffraction simultaions. The quantity $\boldsymbol{n}\varphi_D$ is integrated over the wetted surface.

Wave Spectrum

For the simulations presented here, spectra were produced using the WAFO MATLAB toolbox [8]. Specifically, the Joint North Sea Wave Project (JONSWAP) spectrum was used. The peak period and significant wave height were specified. The concentration factor of the spectrum on the peak frequency was equal to 1, and all other parameters remained at default values.

Time-Domain Hydrodynamic Forces

Irregular waves contain waves that are random in height and period and are often characterized using a wave spectrum that describes the wave energy (wave height) distribution over a range of wave frequencies.

The coefficients returned from WAMIT apply only for monochromatic sea states. In order to effectively simulate irregular waves, it is necessary to apply an irregular excitation force and an irregular radiation force. The irregular excitation force can be written as the real part of an integral term in frequency,

$$\boldsymbol{F_{ex}}(t) = \Re\left(\int_0^\infty \sqrt{2S(\omega)}\boldsymbol{FX}(\omega)e^{i(\omega t+\phi)}d\omega\right) \tag{4}$$

where $\Re$ denotes the real part of the argument, S is the wave spectrum, and ϕ is a random phase. The irregular radiation term can be accounted by the following equation,

$$\boldsymbol{F_{rad}}(t) = -A_\infty \ddot{\boldsymbol{X}} - \int_0^t \boldsymbol{K}(t-\tau)\dot{\boldsymbol{X}}(\tau)d\tau \tag{5}$$

where A_∞ is the added mass at infinite frequency, $\dot{\boldsymbol{X}}$ is the velocity of the body, $\boldsymbol{K}$ is the impulse response function (IRF). The IRF is defined in terms of the radiation damping coefficients [7],

$$\boldsymbol{K}(t') = \frac{d}{dt'}\left(\frac{2}{\pi}\int_0^\infty \frac{B_{ij}(\omega)}{\omega}\sin(\omega t')\,d\omega\right) \tag{6}$$

WEC PTO System Dynamics

The two-body floating-point absorber is designed to generate power from the relative motion between the floating body and the submerged body. In addition, the floating part is only allowed to move along the central column of the submerged body. Therefore, we represented the PTO mechanism as a linear spring-damper system, where the generated power was proportional to the relative translational motion and velocity,

$$\boldsymbol{F_{PTO}} = -k_{lin}\boldsymbol{X_{rel}} - c_{lin}\dot{\boldsymbol{X}}_{\boldsymbol{rel}} \tag{7}$$

where k_{lin} is the stiffness of the system, c_{lin} is the damping coefficient, $\boldsymbol{X_{rel}}$ and $\dot{\boldsymbol{X}}_{\boldsymbol{rel}}$ are the relative motion and velocity between the two bodies.

Viscous Damping

Generally, the effect of viscosity on the system dynamics of a point absorber WEC device needs to be considered, and neglecting that may lead to overestimate the power generation performance of the system, particularly when a linear model is applied. A common way of modeling the viscous damping effect is to add a quadratic damping term to the equation of motion,

$$\boldsymbol{F_V} = 0.5 C_d \rho A_d |\dot{\boldsymbol{X}}|\dot{\boldsymbol{X}} \tag{8}$$

where C_d is the viscous drag coefficient, and A_d is the characteristic area. However, the viscous damping coefficient for the device needs to be carefully selected [9].

NUMERICAL IMPLEMENTATIONS

The WEC was numerically modeled in two distinct phases. First, WAMIT was utilized to calculate a potential theory solution that was used to produce hydrodynamics coefficients. These coefficients along with the buoyancy restoring forces, viscous forces and PTO forces were then converted to time varying forces, which were applied to SimMechanics to solve the system dynamics of the device. This allowed WEC performance characteristics to be estimated. Note that the two-body floating-point absorber predominantly generates energy from the heave motion. Therefore, to simply the problem, only the heave degree-of-freedom was modeled in this study.

Implementation in WAMIT

Frequency-domain hydrodynamic coefficients were extracted from WAMIT by running a simulation with two cylindrical bodies (representing the float and reaction plate of the WEC). The geometry of these bodies is shown in Figure 1.

The radiation and diffraction problems were solved for each body for a range of frequencies. Infinite and 0 frequency cases were also included. For every frequency, added-mass coefficients, radiation damping coefficients, and imaginary and real components of the excitation force were provided. In addition, the F2T function in WAMIT was used to compute the time-domain IRF that describes the response of the body to an impulse force.

Implementation in SimMechanics

In SimMechanics, two bodies were created with the characteristics shown in Figure 1 and Table 1. The relative motion of these bodies was constrained to linear heave motion about a common axis. Those hydrodynamics coefficients obtained from WAMIT were converted to time varying forces (Eqs. 4-5) in discrete form and applied to the system dynamic equation (Eq. 1).

The second term on the right hand side of Eq. 5, also referred to as convolution integral term, represents the fluid memory effect, which characterizes the radiation force induced by the oscillating body motion in time-domain. The fluid memory term includes an integral term from the start of the simulation to the present time t. However, it becomes computationally inefficient as the simulation time becomes longer. A finite value (T_{mem}) for the length of the fluid memory effect can be selected based on characteristics of the IRF. As a result, the fluid memory term will be only integrated from t-T_{mem} *to* t. The impulse response function for motion of the floating body in heave was calculated using the F2T function in WAMIT for a length of 500 seconds (Figure 2).

To determine the length of the fluid memory calculation, a linear estimation was utilized, where the absolute value of the IRF was integrated with time. The integration of the function presented in Figure 2 (the IRF function) is normalized by its maximum value and plotted against time in Figure 3. This function gives some idea of the percentage of the IRF as a function of time. As shown in Figure 3, approximately 80% of the response is captured within the first 10 sec. For this reason, T_{mem} was set at 10 seconds for all the following simulations.

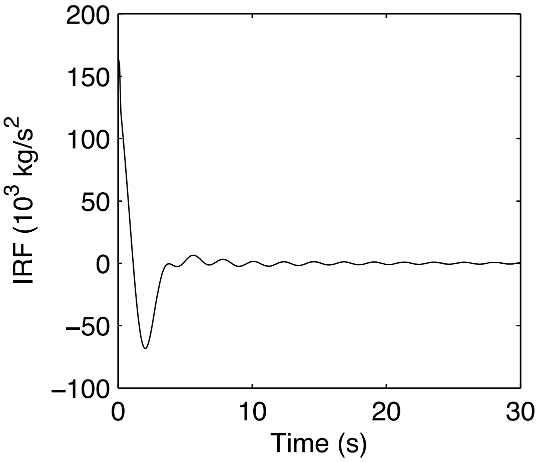

FIGURE 2. IRF FOR THE FLOATING BODY IN HEAVE.

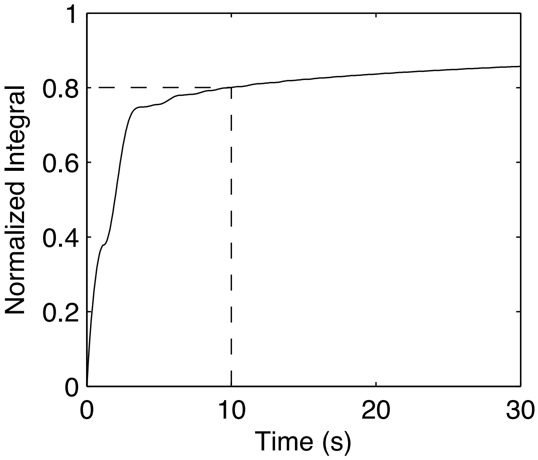

FIGURE 3. NORMALIZED INTEGRAL OF ABSOLUTE VALUE OF IMPULSE RESPONSE FUNCTION.

Buoyant restoring forces were also applied to the bodies. These forces were calculated based on the density and construction of the two bodies. By assuming the displacement is relatively small, linear theory was applied, where the restoring force of the bodies was calculated with respect to the mean free surface.

The system dynamic equation (Eq. 1) for the time-domain simulation was then solved in SimMechanics using a 4th Order Runge-Kutta method for time marching. The time step size is 0.1 sec, and the total length of the simulation is 1000 sec.

Site Specific Power Estimations

Generally, the site-specific average power can be estimated by multiplying the power matrix of the device with the wave scatter diagram at a specific site. The power matrix provides a tabular description of the device power performance for given sea states, which is defined by significant wave height and peak period. The wave scatter diagram, on the other hand, provides the statistical occurrence of the sea states at the site.

$$P_{SS} = \sum_{i,j} P(H_s^i, T_p^j) \cdot JPD(H_s^i, T_p^j) \tag{9}$$

where P_{ss} is the estimated site-specific average power, P is the average power output of the device, JPD is the joint probability distribution of the site, H_s is the significant wave height, and T_p is the peak period.

RESULTS AND DISCUSSION

Verification for Single Body in Heave

In order to verify the developed numerical model, the numerical result was compared to the theoretical solution in a forced harmonic motion problem. The simulation was performed with a single body connected to a fixed reference frame with a linear PTO system (Figure 4). The body had geometry as shown for the top body in Figure 1. Hydrostatic forces, linear radiation damping forces, gravitational forces, PTO forces, and an external forcing function were considered. A sinusoidal forcing function was used.

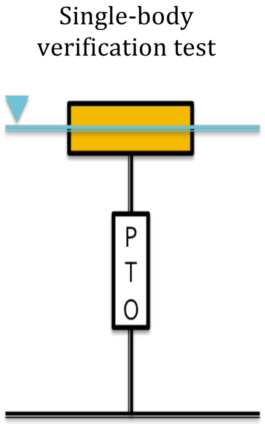

Property	Value
PTO Damping	50 kN-s/m
PTO Spring	5 kN/m
Rad. Damping	100
Body Diam.	11.0 m
Body Height	3.0 m
Body Density	500 kg/m³
Added Mass	10
Force Amp.	10
Force Period	2.0 s

FIGURE 4. SINGLE-BODY VERIFICATION CASE SPECIFICATIONS

The theoretical solution was calculated for an under-damped harmonically forced spring-mass-damper system [11]. The corresponding spring coefficient, damping coefficient and mass of the system were defined according to the numerical simulation, and the system was forced with the same function as that used in the numerical simulation. The time-varying displacement of the body from both the theoretical and numerical calculations is shown in Figure 5, and the results match perfectly.

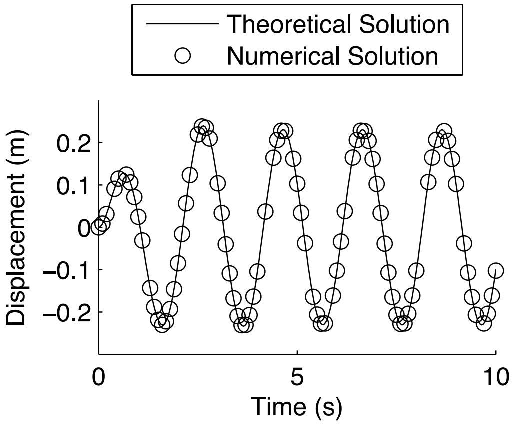

FIGURE 5. DISPLACEMENT HISTORY FOR SINGLE BODY SOLUTION

Grid Resolution Study

A convergence study on the mesh resolution of the float (the upper body shown in Figure 1) was performed in WAMIT. Only the coefficient corresponding to radiation damping for motion of a single body in heave was considered. The number of vertices in the surface mesh was varied between 200 and 3100. The percent different from the coefficient obtained with 3100 vertices is shown for three different periods in Figure 6, Figure 7, and Figure 8.

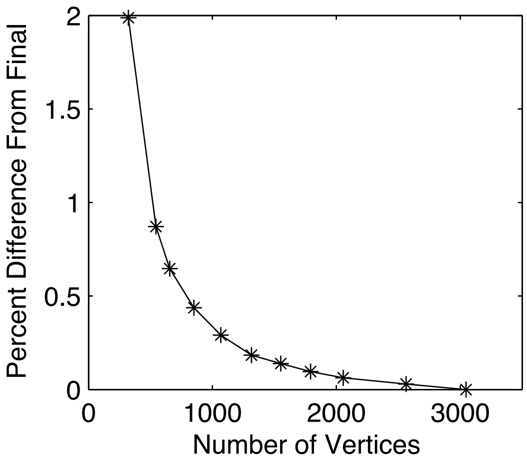

FIGURE 6. CONVERGENCE OF NONDIMENSIONAL RADIATION DAMPING COEFFICIENT FOR A 6.0 SECOND PERIOD.

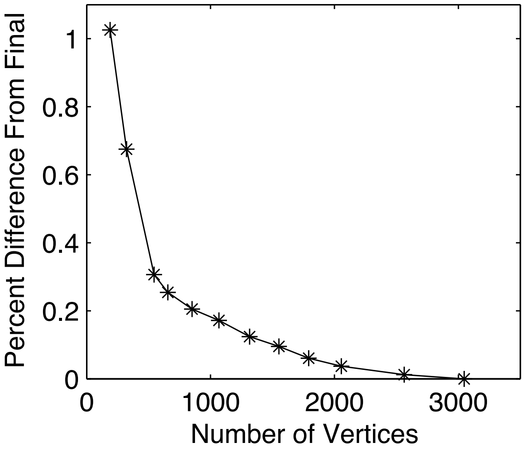

FIGURE 7. CONVERGENCE OF NONDIMENSIONAL RADIATION DAMPING COEFFICIENT FOR A 12.0 SECOND PERIOD

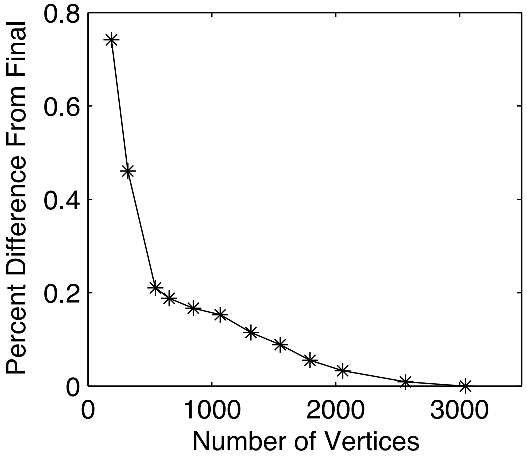

FIGURE 8. CONVERGENCE OF NONDIMENSIONAL RADIATION DAMPING COEFFICIENT FOR A 18.0 SECOND PERIOD

For mesh with more than 1000 vertices, the percent difference fell well below 0.5% for all periods observed. For this reason, the mesh in the following WAMIT simulations, including the mesh for the float and the reaction plate, had a resolution at least higher than the 1000 vertices case.

Fluid Memory Effect

The affect of the fluid memory effect is explored in this section. It was accomplished by observing average predicted power output as a function of peak period and significant wave height, for simulations with and without the fluid memory effect. The peak period was varied from 1 to 11 seconds in increments of 1.0 second. This range was chosen because it easily bracketed the maximum power output of the device. The significant wave height was varied from 0.5 to 3.0 meters, in increments of 0.5 meter. Larger waves were not considered because waves larger than the height of the device would likely introduce nonlinear aspects to the system.

Initially, the simulations were conducted without the fluid memory effect. The results from this sweep are show in Figure 9. A maximum power output of 124 kW was observed at a peak period of 6 seconds.

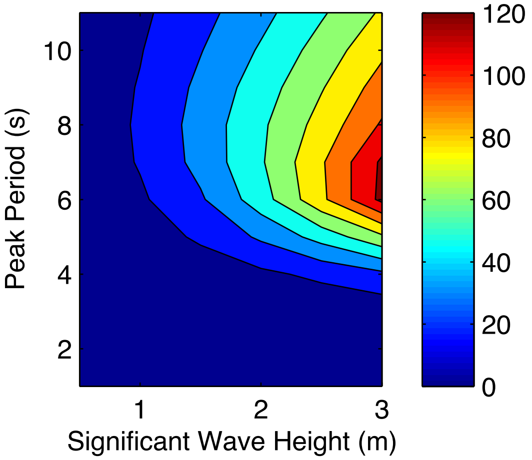

FIGURE 9. POWER MATRIX WITHOUT CONSIDERING FLUID MEMORY EFFECT. UNITS ARE IN KILOWATTS.

A second sweep including the fluid memory effect was performed using the same parameter ranges. The results from this sweep are shown in Figure 10. The maximum value for this sweep was 115 kW, occurring at a peak period of 7 seconds.

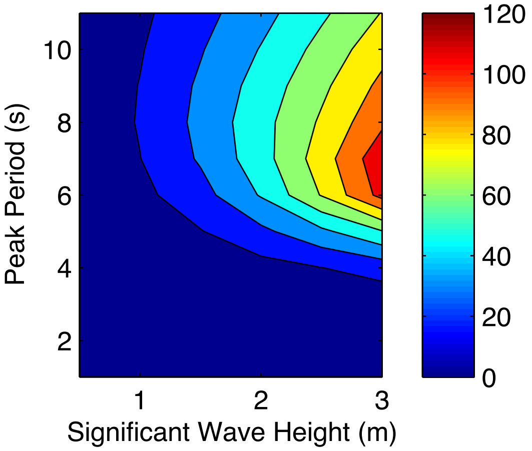

FIGURE 10. POWER MATRIX WITH FLUID MEMORY EFFECT CONSIDERED. UNITS ARE IN KILOWATTS.

For every simulated wave state, the device produced less energy when the fluid memory effect was considered. The percent decrease for all wave states is shown in Figure 11. The effect of fluid memory appeared to be nearly independent of significant wave height, varying mostly with respect to peak period. Although the hydrodynamics are linear, the non-linear multi-body solver causes the slight dependence of percent decrease in power on wave height that is seen in Figure 11.

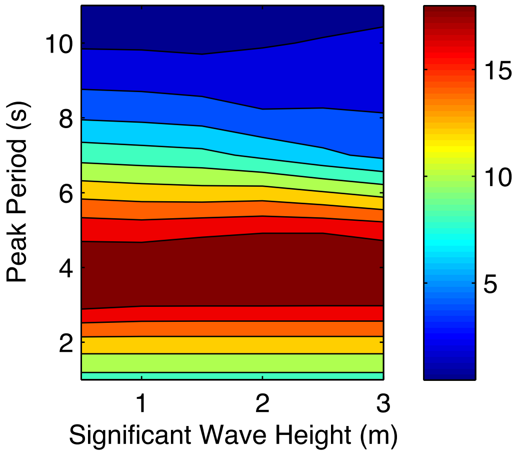

FIGURE 11. PERCENT DECREASE IN POWER OUTPUT WITH INCLUSION OF FLUID MEMORY EFFECT.

Recall that the fluid memory effect is calculated as a convolution integral of the velocity history and the IRF. The Fast Fourier Transform (FFT) of the IRF in Figure 2 is provided in Figure 12. The largest magnitude frequency in the FFT is 0.21 Hz, which corresponds to a period of 4.6 s. This coincides quite closely with the location of the strongest band in Figure 11.

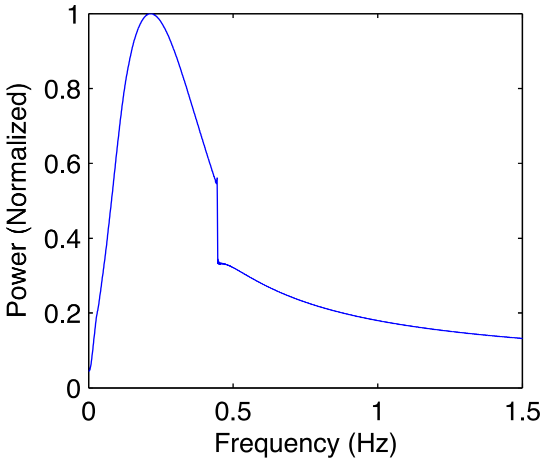

FIGURE 12. FAST FOURIER TRANSFORM OF IRF OF THE FLOAT.

When the float is forced near a period of 4 seconds, the float's velocity history also has a period of around 4 seconds. This matches up closely with the largest magnitude period of the float IRF, where the incident wave period is close to the resonant period of the float. As a result, the fluid memory effect, representing the effect of wave radiation due to the floating oscillation on the system dynamic response, becomes more important on the system power performance. The result causes the strong band around 4 sec that is observed in Figure 11.

Example of Site Specific Power Estimations

Knowing the predicted power output of the device for different wave states allows us to perform site-specific power estimates. Hanstholm, Denmark will be used as a potential site for this example. The wave scatter diagram for this location is shown in Figure 13 [12].

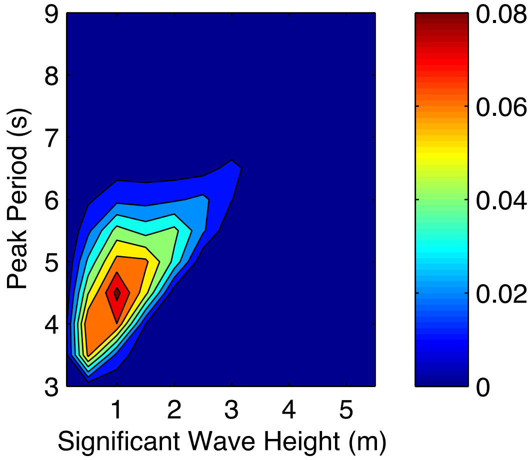

FIGURE 13. WAVE SCATTER DIAGRAM (JOINT PROBABILITY) FOR HANSTHOLM.

The site-specific average power output at the Hanstholm site was calculated with and without the consideration of the fluid memory effect. The calculation was conducted by multiplying the wave scatter diagram (Figure 13) with the power matrix of the device (Figure 9 and Figure 10). The predicted power performance and the required computational time are listed in Table 2. Note that each power matrix was obtained from 66 simulation runs, which were defined by 6 significant wave heights and 11 peak periods. T_{NF} is the simulation time for each run in the case without the consideration of fluid memory effect. The results revealed that neglecting the fluid memory term could reduce the computational time by half but also lead to overestimate the annual averaged site-specific energy production by 15% in this example case. Note that the results are expected to be site specific, which may depend on the peak period of the waves and the resonant period of the float.

TABLE 2. RESULTS OF SITE SPECIFIC AVERAGE POWER PREDICTIONS.

Method	Power Prediction	Computation Time
With FME	14.44 kW	$66T_{NF}$
Without FME	12.32 kW	$132T_{NF}$

CONCLUSIONS

This work demonstrates that time-domain analysis can be implemented using WAMIT and SimMechanics. Since SimMechanics interfaces easily with Simulink, this work offers an easily extendable platform for examining nonlinear control strategies, nonlinear PTO models, and other complex WEC-fluid interaction calculations.

This work also investigated the effect of fluid memory on predict power output. For the device simulated, it was observed that neglecting the fluid memory made a large impact on power output predictions and the percent decrease in power output caused by the inclusion of fluid memory was generally independent of wave height. However, further investigation is needed to determine if this relationship holds true for other types of WEC devices.

The work also provided a preliminary study on the development of time-domain numerical models for simulating WEC devices. NREL is collaborating with Sandia National Laboratory to continue the development of WEC simulation capabilities using the SimMechanics framework. The tool will include the capability to model a wide range of WEC devices that are comprised of multiple bodies, PTO systems, and mooring systems. The code will be made available to the research community in an open-source format in the second half of 2014.

ACKNOWLEDGEMENTS

This work was completed with support from the Department of Energy and the National Renewable Energy Lab.

REFERENCES

[1] Drew, B., Plummer, A.R., and Sahinkaya, M.N., 2009, “A Review of Wave Energy Converter Technology,” Proc. IMechE, 223, pp. 887-901.

[2] Mørk, G., Barstow, S., Kabuth, A., Pontes, M.T., 2010, “Assessing the Global Wave Energy Potential”, Proceedings of 29th International Conference on Ocean, Offshore Mechanics and Arctic Engineering.

[3] Czech, B. and Bauer, P., 2012, “Wave Energy Converter Concepts: Design Challenges and Classification”, Industrial Electronics Magazine IEEE, pp. 4-16.

[4] Li, Y. and Yu, Y., 2012, “A Synthesis of Numerical Methods for Modeling Wave Energy Converter-Point Absorbers,” Renewable and Sustainable Energy Reviews, 16 (6), pp. 4352–4364.Bosma, B., Zhang, Z., Brekken, T.K.A., Ozkan-Haller, H.T., McNatt, C. and Yim, S.C., 2012, “Wave Energy Converter Modeling in the Frequency Domain: A Design Guide”, Proceedings of the Energy Conversion Congress and Exposition, pp. 2099-2106.

[5] Bachynski, E., Young, Y.L. and Yeung, R.W., 2012, “Analysis and optimization of a tether wave energy converter in irregular seas”, Renewable Energy, 48, pp. 133-145.

[6] Cummins, W., 1962, “The Impulse Response Function and Ship Motions”. David Taylor Model Dasin - David W. Taylor Naval Ship Research and Development Center.

[7] “WAMIT User Manual, Version 6.4”, 2006, WAMIT Inc., Chestnut Hill, MA.

[8] WAFO-group, 2000, "WAFO - A Matlab Toolbox for Analysis of Random Waves and Loads - A Tutorial" Math. Stat., Center for Math. Sci., Lund Univ., Lund, Sweden. URL: http://www.maths.lth.se/matstat/wafo.

[9] Babarit, A., Hals, J., MUliawan, M.J., Kurniawan, A., Moan, T. and Krokstad, J., 2011, “Numerical benchmarking study of a selection of wave energy converters”, Renewable Energy, 41, pp. 44-63.

[10] Falcao, A.F. de O., 2009, “Wave energy utilization: A review of the technologies,” Renewable and Sustainable Energy Reviews, 14, pp. 899-918.

[11] Inman, D. J., 2001, *Engineering Vibration*, Prentice Hall, Upper Saddle River, NJ

[12] RAMBOLL and LNEG. “ANNEX II: Task 1.1 Generic and Site-related Wave Energy Data”, www.ocean-energy-systems.org, 2010